



Article

Mapping Land Use/Cover Dynamics of the Yellow River Basin from 1986 to 2018 Supported by Google Earth Engine

Qiulei Ji ¹, Wei Liang ^{1,2,*}, Bojie Fu ³, Weibin Zhang ⁴, Jianwu Yan ¹, Yihe Lü ³, Chao Yue ⁵, Zhao Jin ⁵, Zhiyang Lan ¹, Siya Li ¹ and Pan Yang ¹

- ¹ School of Geography and Tourism, Shaanxi Normal University, Xi'an 710119, China; thrillerlemon@snnu.edu.cn (Q.J.); yanjw@snnu.edu.cn (J.Y.); zhiyang1998@snnu.edu.cn (Z.L.); lee9741@snnu.edu.cn (S.L.); panyang@snnu.edu.cn (P.Y.)
- ² National Demonstration Center for Experimental Geography Education, Shaanxi Normal University, Xi'an 710119, China
- ³ Research Center for Eco-Environmental Sciences, State Key Laboratory of Urban and Regional Ecology, Chinese Academy of Sciences, Beijing 100085, China; bfu@rcees.ac.cn (B.F.); lyh@rcees.ac.cn (Y.L.)
- ⁴ Xi'an Gu Bo Electronic Intelligent Technology Co., Ltd., Xi'an 710119, China; wbzhang@snnu.edu.cn
- ⁵ State Key Laboratory of Soil Erosion and Dryland Farming on the Loess Plateau, Northwest A&F University, Yangling 712100, China; chaoyuejoy@gmail.com (C.Y.); jz1989@nwafu.edu.cn (Z.J.)
- * Correspondence: liangwei@snnu.edu.cn; Tel.: +86-29-8531-0525

Abstract: Changes in the land use/cover alter the Earth system processes and affect the provision of ecosystem services, posing a challenge to achieve sustainable development. In the past few decades, the Yellow River (YR) basin faced enormous social and environmental sustainability challenges associated with environmental degradation, soil erosion, vegetation restoration, and economic development, which makes it important to understand the long-term land use/cover dynamics of this region. Here, using three decades of Landsat imagery (17,080 images) and incorporating physiography data, we developed an effective annual land use/cover mapping framework and provided a set of 90 m resolution continuous annual land use/cover maps of the YR basin from 1986 to 2018 based on the Google Earth Engine and the Classification and Regression Trees algorithm. The independent random sampling validations based on the field surveys (640 points) and Google Earth (3456 points) indicated that the overall accuracy of these maps is 78.3% and 80.0%, respectively. The analysis of the land system of the YR basin showed that this region presents complex temporal and spatial changes, and the main change patterns include no change or little change, cropland loss and urban expansion, grassland restoration, increase in orchard and terrace, and increase in forest during the entire study period. The major land use/cover change has occurred in the transitions from forests, grasslands, and croplands to the class of orchard and terrace (19.8% of all change area), which not only increase the greenness but also raised the income, suggesting that YR progress towards sustainable development goals for livelihood security, economic growth, and ecological protection. Based on these data and analysis, we can further understand the role of the land system in the mutual feedback between society and the environment, and provide support for ecological conservation, high-quality development, and the formulation of sustainable management policies in this basin, highlighting the importance of continuous land use/cover information for understanding the interactions between the human and natural systems.

Keywords: Google Earth Engine; Landsat; land use/cover change; Loess Plateau; Yellow River basin



Citation: Ji, Q.; Liang, W.; Fu, B.; Zhang, W.; Yan, J.; Lü, Y.; Yue, C.; Jin, Z.; Lan, Z.; Li, S.; et al. Mapping Land Use/Cover Dynamics of the Yellow River Basin from 1986 to 2018 Supported by Google Earth Engine. *Remote Sens.* **2021**, *13*, 1299. <https://doi.org/10.3390/rs13071299>

Academic Editor: Jordi Cristóbal Rosselló

Received: 21 February 2021
Accepted: 19 March 2021
Published: 29 March 2021

Publisher's Note: MDPI stays neutral with regard to jurisdictional claims in published maps and institutional affiliations.



Copyright: © 2021 by the authors. Licensee MDPI, Basel, Switzerland. This article is an open access article distributed under the terms and conditions of the Creative Commons Attribution (CC BY) license (<https://creativecommons.org/licenses/by/4.0/>).

1. Introduction

A long-standing global challenge for achieving sustainable development is how to satisfy the ever-growing demands of humans while maintaining the integrity of ecosystems [1]. Land use/cover is an important source of information to understand the complex interaction between human activities and the ecological environment [2], which is both

the cause and consequence of global environmental change [3,4]. The transformation of the Earth's biosphere is reflected in the change of the land system, which is considerably altering Earth system processes, including surface energy balance [5], water cycle [6], and the carbon cycle [7]. As the growing global population and more requires of forestry and agricultural products, the intense land use/cover changes (LUCC) driven by human activities will further intensify, which will put tremendous pressure on the structure and function of ecosystems as well as the provision of ecosystem services [8,9]. Meanwhile, the demand for land-based harvestable biomass (e.g., food, fuel, and fiber) will surge in the coming decades [10], which is the challenge of managing trade-offs between maintaining the capacity of the ecosystem and human needs [3,11]. Therefore, a better understanding of the long-term gradual changes in land use/cover is critical to advance our knowledge of global sustainability and the coupled human-nature system.

As the fastest growing economy in the world, China has 18% of the world's population [12]. Recent research reports that China and India led in global greening through land-use management [13]. The increase in leaf area of China was mainly from forests and croplands. Thanks to the implementation of large-scale ecological conservation and restoration programs by the government, The Huang He, or Yellow River (YR) basin and particularly its middle parts (the Loess Plateau) exhibited the largest vegetation greening trend in China [14,15]. The YR basin is an important ecological corridor in China but with a fragile ecological environment and severe rural poverty, which is a global hotspot of competition between human and natural systems and it is suffering from soil erosion and environmental degradation [16]. With the combined effects of environmental factors, ecological conservation programs, and socio-economic, the vegetation cover and land use/cover of this arid and semiarid area experienced a dramatic transformation [17,18]. In recent years, with great pressure from rapid population rise, resource consumption, and environmental change, the dynamic changes of social systems and ecological systems have become more intensive and complex. The potential competition between ecosystems and humans also has become increasingly fierce, which seriously threatens the sustainable development of this region [19–21]. However, the long-term change process of the environmental pattern in the YR basin is still not clear, and the implementation effects of environmental conservation programs also need long-term monitoring and evaluation. It is highly desirable to generate continuous time series of LUCC information to reveal the change process and characteristics of the land system of the YR basin.

In fact, there are already many land use/cover products, which have been applied to different fields in the YR basin. As listed in Table S1, most of the previous studies on the YR basin used a fixed (single) or short time period of the land use/cover map. Although several global land use/cover products exist, these data products cannot have a high spatial resolution at the same time as high temporal resolution, and vice versa. In the past three decades, the YR basin has witnessed large-scale environmental damage and restoration, which deeply affected the regional land-system [18,22]. More importantly, the YR basin has large terrain undulations and strong surface heterogeneity which affect the trend of LUCC and the response of the ecological system a lot [23,24]. Research on the relevant processes of the basin puts forward higher requirements on the continuity and accuracy of the data. On the other hand, the classification strategy and scheme with existing data cannot accurately describe the transformation of special land features in this area, and a spatially explicit assessment and optimization for ecosystem services based on land use/cover management cannot be achieved feasibly.

The objectives of this study are: (1) provide a set of continuous annual land use/cover maps of the YR basin; (2) analyze land use/cover dynamics, and discuss the characteristics and potential causes of LUCC; (3) evaluate the effects of environmental conservation programs such as the Grain for Green (GFG) program [25] and discover the environmental crisis that may be hidden behind LUCC. These maps produced by this study can provide a research basis for other key scientific issues related to land system and ecological environment changes in the YR basin. Such detailed and multifaceted LUCC analyses can provide

new insights into regional dynamics, which are important for scientists and policy makers for assessing several issues associated with environmental sustainability and human and natural systems.

2. Materials and Methods

2.1. Study Area

The YR, the cradle of Chinese civilization, is a major source of freshwater for approximately 107 million people and consists of 12.6 million hectares of cultivated land which provide 18% of the food production in China [26]. The main crops planted in the YR basin are wheat and maize, some soybeans and rice are also planted. It has complicated landforms which comprise mountains, basins, sub-plateaus, gullies, hills, and alluvial plains ranging in elevation from -52 to 6254 m. This basin is characterized by a continental climate, with a subordinate arid climate in the western part, a semiarid climate in the middle part, and a semi-humid climate in the eastern part. Due to various landforms and climate types, the YR has formed many ecosystems suitable for numerous kinds of life and vegetation. The Loess Plateau, the middle part of the YR basin, is one of the four major plateaus in China. This region is an important energy (e.g., coal, gas, and oil) and chemical industry base in North China. As a result of thousands of years of soil erosion and environmental problems, 70% of the Loess Plateau has become a region dominated by hills and gullies. To mitigate serious environmental problems, a series of conservation programs, such as the GFG program and the Natural Forest Conservation (NFC) program [27], have been widely implemented within this region by the Chinese government. These programs have greatly altered the landscape, with the vegetation cover on the Loess Plateau having doubled from 1999 to 2013 (31.6% to 59.6%) [14].

The study area combines the boundaries of the YR basin and the entire Loess Plateau with a buffer zone of 10 km, and the total area of the whole region is $967,000$ km² or roughly one-tenth of the territory of China (Figure 1). The YR basin is critical for China's socio-economic development as well as ecosystem conservation. Over the past few decades, the economy, population, and grain production of the YR basin have all increased rapidly. In the context of drastic human activities and climate change, the YR basin has also witnessed regional greening and reduction of runoff and sediment (Figure 1). These changes not only put great pressure on the land system of the YR basin, but also brought huge challenges to the managers of the area in guaranteeing the security of food, energy, and water. Therefore, the study area needs detailed information about the land use/cover dynamic to promote conservation of the ecosystem and improve people's lives in this water-limited region.

2.2. Methods and Data in Google Earth Engine

Aiming at the production of continuous annual land use/cover data, this study proposed an effective land use/cover classification framework, including Landsat data filtering and anomalous data repair methods, feature variable selection, result optimization, and assessment strategies. The entire workflow was based on the Google Earth Engine (GEE) platform, including data preprocessing, annual land use/cover data production, and LUCC analysis (Figure 2). The data used were mainly from filtered and repaired Landsat data which included six spectral bands (i.e., blue, green, red, near infrared, shortwave infrared 1, shortwave infrared 2), and digital elevation data of Shuttle Radar Topography Mission (SRTM) [28] (with variables elevation, slope, and topographic diversity). Besides, four spectral indices calculated based on Landsat data were also added to improve the classification performance. We chose the Classification and Regression Trees (CART) [29] as the classification method. Through space-time optimizing strategy, the time series of the mapping results were optimized and smoothed. Finally, after validation, the continuous annual land use/cover of the YR basin was produced. Then, the land use/cover transition matrix and transition network were used to analyze the spatiotemporal changes and transition characteristics of various land use/cover classes in this basin during the past 33 years.

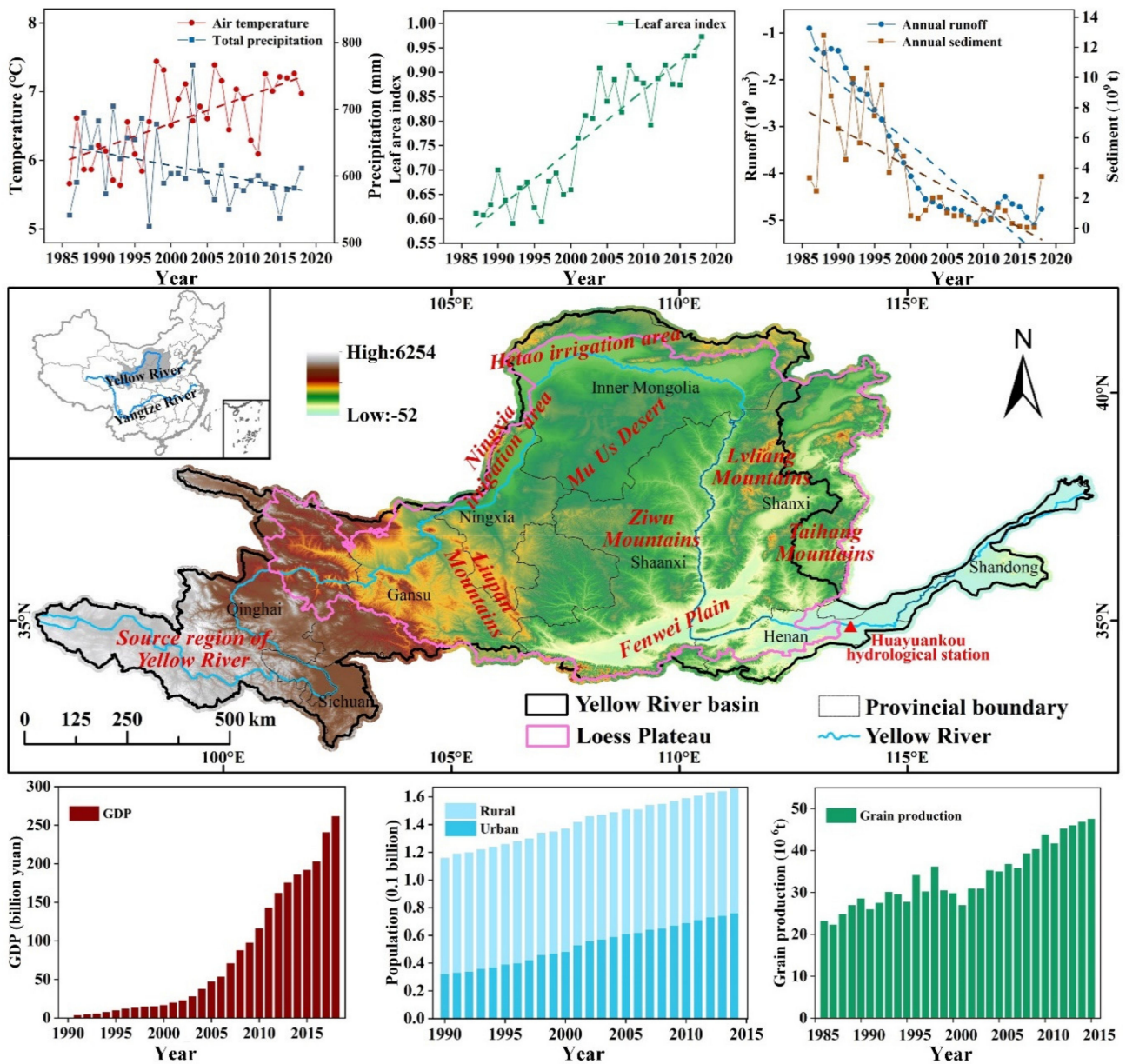


Figure 1. Location of the Yellow River basin and the Loess Plateau. The data source of average temperature and the average total precipitation of the study area is ERA5 (the fifth generation European Centre for Medium-Range Weather Forecasts atmospheric reanalysis of the global climate). The data source of the average leaf area index of the study area is AVHRR (Advanced Very High-Resolution Radiometer). The total runoff and total sediment data are from the statistical data of the Huayuankou hydrological station (the boundary between the middle and lower reaches of the YR). The data of the regional sum of Gross Domestic Product (GDP), population, and grain production come from the statistical yearbook.

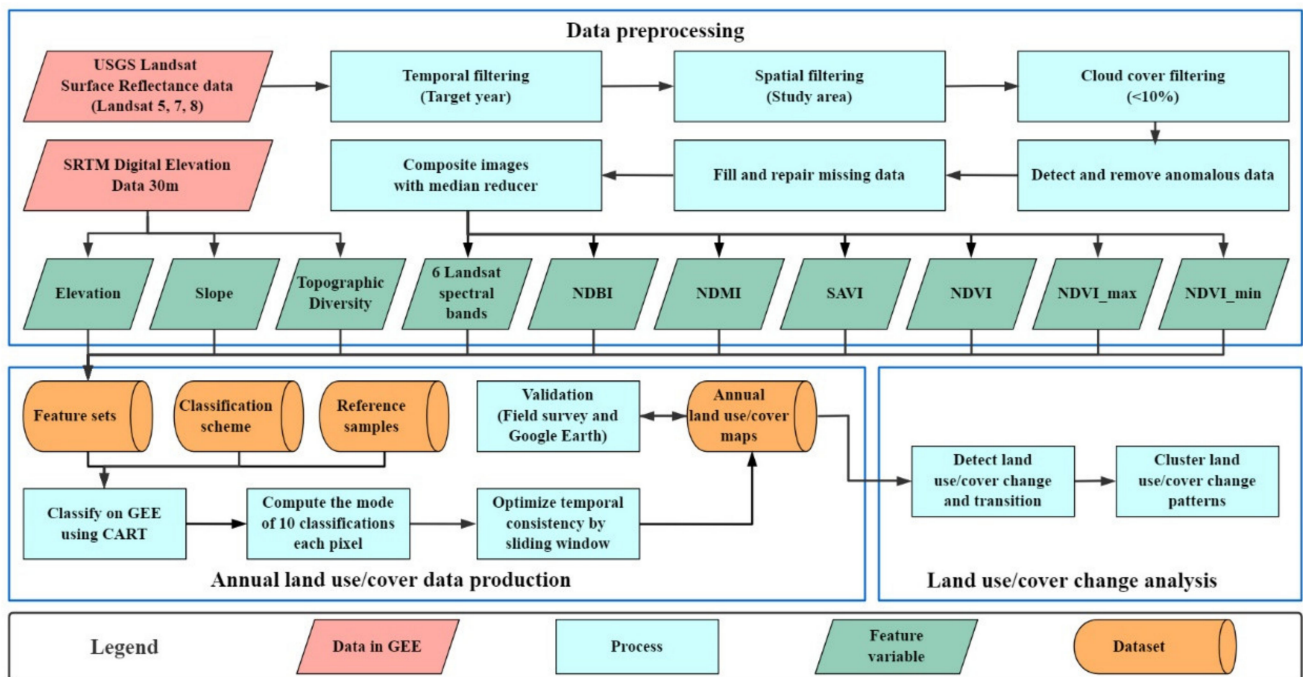


Figure 2. Workflow for the long-term annual land use/cover production and land use/cover change analysis in this study. Major modules include data preprocessing, annual land use/cover data production, and land use/cover change analysis.

GEE is a planetary-scale database and data processing platform driven by Google Cloud Computing, which contains petabyte-scale remote sensing images and geoscientific datasets. Meanwhile, it has planetary-scale processing capabilities, providing researchers and developers with a convenient and fast platform for data acquisition, processing, and analysis [30]. Therefore, GEE provides a powerful tool for data-driven scientific research and has been widely used to monitor the changes in land use/cover in a single class such as forest [31,32], cropland [33,34], water body [35,36], and urban [37,38] or all land use/cover classes [39,40] over many areas around the world or for the entire globe. This study used 33 years of historical Landsat images and other auxiliary datasets to map the annual land use/cover of the YR basin during 1986–2018 (Table 1).

Table 1. Datasets used in this study. All are available on the GEE platform. USGS represent United States Geological Survey.

Dataset	GEE ID	Dataset Provider	Period	Spatial Resolution
USGS Landsat 5 Surface Reflectance Tier 1	LANDSAT/LT05/C01/T1_SR	USGS	1986–2011	30 m
USGS Landsat 7 Surface Reflectance Tier 1	LANDSAT/LE07/C01/T1_SR	USGS	2012	30 m
USGS Landsat 8 Surface Reflectance Tier 1	LANDSAT/LC08/C01/T1_SR	USGS	2013–2018	30 m
SRTM Digital Elevation Data	USGS/SRTMGL1_003	NASA/USGS/JPL-Caltech	2000	30 m
Global SRTM Topographic Diversity	CSP/ERGo/1_0/Global/SRTM_topoDiversity	Conservation Science Partners	2000	270 m

The Landsat satellite images provide the longest temporal data of space-based earth surface observations [41]. Due to the failure of the Landsat 7 Scan Line Corrector, all Landsat 7 ETM + images have the problem of data loss gaps and are not directly ready for use after 31 May 2003 [42]. We used surface reflectance data of Landsat 5 from 1986 to 2011, Landsat 7 in 2012, and Landsat 8 from 2013 to 2018, which have been atmospherically corrected using the Landsat Ecosystem Disturbance Adaptive Processing System [43], and include a cloud, shadow, water, and snow mask produced using the C Function of Mask [44]. The SRTM V3 product was provided by the National Aeronautics and Space

Administration (NASA) Jet Propulsion Laboratory (JPL) at a resolution of 1 arc-second and the elevation information can be further calculated to reflect the terrain. Global SRTM Topographic Diversity was based on the 30 m SRTM digital elevation data and represents the variety of moisture and temperature conditions available to species at local habitat, which expresses the theory that a higher variety of topo-climate niches can support species persistence and higher diversity [24]. Combining the long-time series of remote sensing images and these physiography variables can help distinguish different vegetation types growing on the ground with different characteristics.

2.3. Classification Scheme

The land use/cover classification scheme used mainly followed the classes in the International Geosphere-Biosphere Programme (IGBP) classification scheme according to the capability of the data used and the regional features of the YR basin [45] (Table 2). The grassland ecosystem is one of the most important ecosystems of the study area, and there are certain differences in the climatic conditions of grassland distribution. Specifically, most of the grasslands on the Loess Plateau grow in the xeric environments, whereas alpine meadow with high coverage is the main grassland type in the source regions of the YR. Therefore, we divided the grasslands into low, medium, and high coverage grasslands according to the vegetation coverage. Taking into account the widely distributed terraces and large numbers of economic forests (e.g., fruit trees) in the YR basin, our classification scheme has an additional class of orchard and terrace. In other words, we separated agricultural lands into two types, croplands as well as orchard and terrace classes. Finally, the classification scheme in our study defined 15 classes and detailed descriptions of each class can be found in Table 2.

Table 2. The classification scheme of this study.

First-Degree Class	Second-Degree Class	Abbreviation	Description
Forests	Deciduous Broadleaf Forests	DBF	Dominated by deciduous broadleaf trees (canopy > 2 m). Tree cover > 60%.
	Evergreen Needleleaf Forests	ENF	Dominated by evergreen conifer trees (canopy > 2 m). Tree cover > 60%.
	Mixed Forests	MF	Dominated by neither deciduous nor evergreen (24–36% to 50–50% of each) tree type (canopy > 2 m). Tree cover > 60%.
Shrublands	Shrublands	Shrub	Dominated by woody perennials (1–2 m height) > 60% cover.
Grasslands	Low Coverage Grasslands	LCG	Herbaceous plants with low coverage (<30%), usually covered by annuals xerophyte grasslands.
	Medium Coverage Grasslands	MCG	Herbaceous plants with medium coverage (30~60%).
	High Coverage Grasslands	HCG	Herbaceous plants with high coverage (>60%), usually covered by perennial temperate grasslands
Agricultural Lands	Croplands	Crop	Dominated by herbaceous annuals (<2 m). At least 80% cultivated cereal crops.
	Orchard and Terrace	OT	Mosaics of agricultural or artificial vegetation growing on sloping land, including orchards and terraces.
Urban and Built-up	Urban and Built-up	UB	At least 60% of area is covered by building materials, transportation lands, and other impervious surface area.

Table 2. Cont.

First-Degree Class	Second-Degree Class	Abbreviation	Description
Water Bodies	Surface Water	Water	At least 60% of area is covered by water located on top of the Earth's surface.
	Wetlands	Wet	Permanently inundated lands with 30–60% water cover and > 10% vegetated cover.
	Snow and Ice	Snow	At least 60% of area is covered by snow and ice.
Desert and Low-vegetated Lands	Desert and Bare soil	DB	At least 60% of area is covered by desert or bare rock and soil.
	Low-vegetated Lands	LV	At least 60% of area is low-vegetated lands with less than 10% vegetation, such as tundra and saline-alkali soil.

2.4. Classification Method and Strategy

To composite more high-quality and clear images, we filtered out Landsat scenes with high cloud coverage (“Cloud cover filtering” in Figure 2). Finally, 17,080 Landsat scenes (cloud cover percentage less than 10%) were achieved from 1986 to 2018 in the study area (Figure S1). The images used are more distributed in high latitudes (37°N–43°N) than in low latitudes (31°N–37°N), including 12957 scenes Landsat 5, 527 scenes Landsat 7, and 3596 scenes Landsat 8 images. Despite the comparative good quality, anomalies of Landsat still occurred occasionally, which may affect classification results. Here, two types of anomalous data need to be filtered and repaired (“Detect and remove anomalous data” in Figure 2). The first type is the so-called Christmas tree anomaly (Figure S2a). When the image was viewed in 3-band Red Green Blue (RGB) combination, the anomalous data appeared as red, green, and blue pixels at the edge of the image scene. We clipped the anomalous data directly using an inner buffer of 3000 m for each image scene, which will not affect the classification results. The second type of anomalous data is well-known as a caterpillar track (Figure S2b). The first three bands (Blue, Green, and Red) of the caterpillar track were often negative, and some large outliers were found in Band 6 of brightness temperature (B6), which were usually equal to or greater than 20,000. In most cases, the caterpillar tracks run throughout the whole image scene. Therefore, we used the buffer tool to construct an annulus region from −5000 m to −15,000 m (Figure S2c) and obtained the maximum of the B6 of pixels value in the annulus. If this maximum value was greater than 15,000, we marked it as anomalous data and would not use it in the classification. Besides, data gaps may occur for pixels covered by few Landsat scenes when masking cloud and cloud shadow pixels. We also need to fill the gaps of Landsat 7 images. To repair these two cases of missing data (“Fill and repair missing data” in Figure 2), we blended the original data onto an image by applying a morphological mean filter (`ee.Image.blend()` in GEE Application Programming Interface (API)), then, we got the repaired image that not only retained the original data but also filled the gaps (Figure S2d).

Aiming at a sufficient amount of good quality Landsat scenes for classification for a target year, referred to the practice in previous studies [40,46], we choose 24 months as the chosen time window to composite the annual image for the target year (“Temporal filtering” in Figure 2). For the YR basin, we tried six composite methods including simple composite, greenest pixel composite, least-cloudy pixel composite, medoid composite [47], mean composite, and median composite on GEE (Figure S3). Among them, the median composite is a method that has a better effect and saves calculation memory [48] (“Composite images with median reducer” in Figure 2). Median composite is a kind of pixel-based image compositing method that can eliminate the influence of extreme values due to clouds and shadows and can avoid the edge effects between Landsat scenes. 33 annual maps of the study area were composited by all filtered and repaired Landsat scenes using median composite.

Including ancillary environmental data and various spectral indices during the classification has been demonstrated to improve land type mapping accuracy [49,50]. Among them, vegetation indexes such as Normalized Difference Vegetation Index (NDVI) can help the classifier to distinguish vegetation types from the perspective of vegetation phenology [51]. To find appropriate data and spectral indices as feature sets for classification, we combined the Landsat 6 spectral bands with other ancillary data or various spectral indices calculated from the Landsat 6 spectral bands. The accuracy of the classifier was assessed using these data as the feature set in the year 2010. We selected the top 7 combinations of accuracy from 16 combinations to participate in the classification (“Feature variable” in Figure 2), which could improve the classification accuracy (Table S2). Finally, the data or bands involved in the classification included Landsat 6 spectral bands, elevation, slope, topographic diversity, Normalized Difference Built-up Index (NDBI) [52] (Equation (1)), Normalized Difference Moisture Index (NDMI) [53] (Equation (2)), Soil Adjusted Vegetation Index (SAVI) [54] (Equation (3)), NDVI [55,56] (Equation (4)), maximum NDVI (NDVI_max) (95th percentiles of NDVI for each pixel in target years), and minimum NDVI (NDVI_min) (5th percentiles of NDVI for each pixel in target years). The confusion matrix of the final combination classifier (Table S3) proved that these feature sets can distinguish these 15 land use/cover classes well.

$$\text{NDBI} = \frac{R_{\text{shortwave infrared 1}} - R_{\text{near infrared}}}{R_{\text{shortwave infrared 1}} + R_{\text{near infrared}}} \quad (1)$$

$$\text{NDMI} = \frac{R_{\text{near infrared}} - R_{\text{shortwave infrared 1}}}{R_{\text{near infrared}} + R_{\text{shortwave infrared 1}}} \quad (2)$$

$$\text{SAVI} = \frac{R_{\text{near infrared}} - R_{\text{red}}}{R_{\text{near infrared}} + R_{\text{red}} + L} \times (1 + L); (L = 0.6) \quad (3)$$

$$\text{NDVI} = \frac{R_{\text{near infrared}} - R_{\text{red}}}{R_{\text{near infrared}} + R_{\text{red}}} \quad (4)$$

where R represents the surface reflectance of the corresponding Landsat band. In Equation (3), the correction factor (L) values differed with vegetation density. The value of L ranges from 0.25 to 1. The higher the vegetation density has the lower the value of L. According to the vegetation status of the study area, we set L as 0.6.

We selected reference samples evenly distributed within the study area every year. The training sample polygons were manually drawn in GEE and visually judged by the RGB true color composite image of Landsat and high-resolution images in Google Earth, and also referenced the Moderate-resolution Imaging Spectroradiometer (MODIS) Land Cover Type product. In these sample regions, we extracted the values of pixels in the feature set for the classifier’s training. The distribution of these sample polygons in time and class was shown in Figure S4.

To identify the best suitable classification method for land use/cover mapping over the study area, we took the year 2010 as a testing example. The test feature sets included 6 spectral bands of Landsat 5 and 977 reference sample regions. To assess the accuracy of the classifier, 80% of the reference samples were used for training and the remaining 20% were used for validation. The classification methods involved in testing can be used directly in GEE (Table S4). The Random Forest and the Support Vector Machine were not available for classification work because of the large study area (~1 million km²) and more classes (15 classes), and the user memory limitations which usually resulted into the internal server error of GEE. By comparing the accuracy of different classification methods, the CART, which saves user memory and has higher accuracy, was chosen as our classifier [57]. The CART classifier is formed by the collection of rules based on variables in the dataset and produces either classification or regression trees, depending on whether the dependent variable is continuous or categorical, respectively. The CART classifier constructs a prediction model from the training data, partitions the data space recursively, fits each partition prediction model to predict continuous test variables and target variables,

and obtains a decision tree model. Aiming at avoiding the over-fitting problem in the classification process, the CART algorithm uses cross-validation to prune the decision tree. If the branch maintains a low error rate, it is retained, otherwise, it is deleted, and finally, an optimal binary tree that takes into account the complexity and the error rate is obtained. In each year's classification, we use random 80% of the reference samples to participate in training, and the remaining 20% is used to verify the training accuracy of the classifier.

In order to optimize the land use/cover classification results, we used the classifier to execute classification 10 times for each year and composited these 10 maps using a reducer that computes the mode of the inputs (`ee.Reducer.mode()` in GEE API). This was taken to get 1 annual map from the 10 runs. The main purpose of this operation is to eliminate the uncertainty of the CART method. Next, to adjust temporal consistency, we used the sliding window in the multi-year time series of classification results which will update the focal year's land use/cover class label to the mode values of the class label time series for the time period. We tested the 3 and 5-year sliding windows with reference samples in 33 years and found the 5-year sliding window was more effective (Figure S5). By using this approach, we smoothed the time series of the mapping results to avoid noise interference as much as possible. Finally, we created the optimized annual land use/cover map series of the YR basin (Processes of "Annual land use/cover data production" in Figure 2).

2.5. Data Assessment and Analysis

The annual land use/cover maps of the YR basin were assessed using two independent validation points sets ("Validation" in Figure 2). First, we collected field survey data during 2015, 2017, 2018, and 2019 with 640 ground samples totally which were mainly from Shaanxi, Shanxi, Inner Mongolia, and Ningxia province (Figure S6). Second, given that the long-term field data for validating historical LUCC are hard to obtain, we used the stratified random sampling approach to collect 3456 validation samples from high-resolution historical images in Google Earth, which is a practical sampling method that can satisfy most of the accuracy assessment objectives and the desirable design criteria [58,59]. Limited by the initiation of the commercial era of high spatial resolution satellites (approximately 2000), high-resolution remote sensing images before 2001 are difficult to obtain. Therefore, we performed a stratified random sampling validation on the last 18 LUCC maps which will have small standard errors in the accuracy and area estimates and benefit a full-scale accuracy assessment of the maps [58,59]. 600 validation points were selected in 2018 due to the ease of obtaining high-resolution images in this year. In 2001–2017, a stratified random sampling with the following criteria was designed:

1. Independent sampling: Validation sample points are created independently from training data. All validation points are visually interpreted manually according to the high-resolution images of the corresponding year. If there is no high-resolution image in the corresponding year, refer to the high-resolution image near this point in time or the Landsat image of the corresponding year.
2. Random sampling: Each validation points of each year are spatially independent and randomly distributed in the study area.
3. Stratified sampling: The sample unit for the validation sample was a pixel of 90-m resolution. The sample size was designed to be 168 validation points per year, and a certain number of points will be selected in each class.
4. Balanced sampling: Stratified sampling with proportional allocation balances the proportion of each land use/cover class sample to close to the proportion of the area of each class from the map to be validated. To compromise between favoring user's versus producer's and overall accuracies, we increased the sample size in the rarer classes (No less than 85 per class, that is no less than 5 points per class per year). Finally, 2856 samples (168×17) were sampled in 17 years.

Meanwhile, our land use/cover map was compared with the seven existing land use/cover products in the first-degree classes (Table S5), including forests, shrublands, grasslands, agricultural lands, urban and built-up, water bodies, and desert and low-

vegetated lands. We statistically compared the total area of each land use/cover class in the study area and selected a region covered by multiple classes of land use/cover in the middle reaches of the YR basin to compare the spatial differences in detail.

The land use/cover dynamic detection and analysis methods used in this study mainly include the following:

1. Statistics of the area of each land use/cover class. Use the “`ee.Image.pixelArea()`” in GEE API to implement the area calculation using equal-area projection.
2. Construction of land use/cover transition matrix and transition network between multiple maps. Implement transition type mask extraction and area statistics in GEE.
3. Detection method of area ratio change trend in grids. Use ridge regression to obtain the changing trend in the area ratio of each grid (0.5°) for each class. Furthermore, use the k means algorithm to cluster these change trends, and get several types of LUCC patterns in the study area.
4. Drawing of the spatiotemporal map of land use/cover classes transition. Display the temporal and geographical distribution of land class transition on the map.

3. Results

3.1. Annual Mapping Results and Assessment

The land use/cover mapping result of the YR basin in 2018 is shown in Figure 3a. During the study time period, the dominant land use/cover class was grasslands, including the high coverage grasslands (18.8%) in the headwaters of the YR basin, the medium coverage grasslands (12.5%) in the northwestern part of the study area, and the arid low coverage grasslands (11.6%) in the middle of the Loess Plateau (Figure 3a,b). This was followed by agricultural lands, which were mainly distributed on the plains and hillsides bordering the plains, with croplands and orchard and terrace accounting for 14.78% and 14.78% of the total area, respectively.

Among 33 maps, the performance of the classifiers was stable, and the mean training accuracy of these classifiers was 0.9031 (Figure S7). The mean training accuracy before 2001 was 0.8967. After 2000, the mean training accuracy was 0.9084 which higher than before 2001. We counted the number of land use/cover class unique values in 10 classifications for each pixel each year and 95.25% of the pixels were distributed between 1 and 2 (Figure S8), indicating that the classifiers were robust within most of the study area.

The year and class distribution of these 4096 validation points were shown in Figure 4a,b. The overall accuracy of the 640 field validation point set is 78.3%. Due to their uneven distribution of space and classes, they cannot be used to accurately assess these maps. Therefore, the following confusion matrix analysis is only for the remaining 3456 validation points collected from Google Earth. The validation results indicated that this data set achieved an overall accuracy of 80% for the second-degree classification scheme (15 land use/cover classes). The confusion matrix showed that the classifier performed better in evergreen needleleaf forests, high coverage grasslands, and mixed forests (F1-score were 0.94, 0.92, and 0.90, respectively) but a slightly worse performance for the urban and built-up, orchard and terrace, and low coverage grasslands classes (F1-score were 0.55, 0.73, and 0.74) (Table 3 and Figure S9). There were some misclassifications between croplands, orchard and terrace, and urban and built-up, which are all classes that are relatively affected by human activities. Besides, orchard and terrace were easily misclassified to deciduous broadleaf forests because they may be both planted with deciduous vegetation and mostly distributed on the hillside. Low coverage grasslands were easily misclassified to croplands because the spectral characteristics of herbaceous plants with low coverage were similar to farmland after harvest.

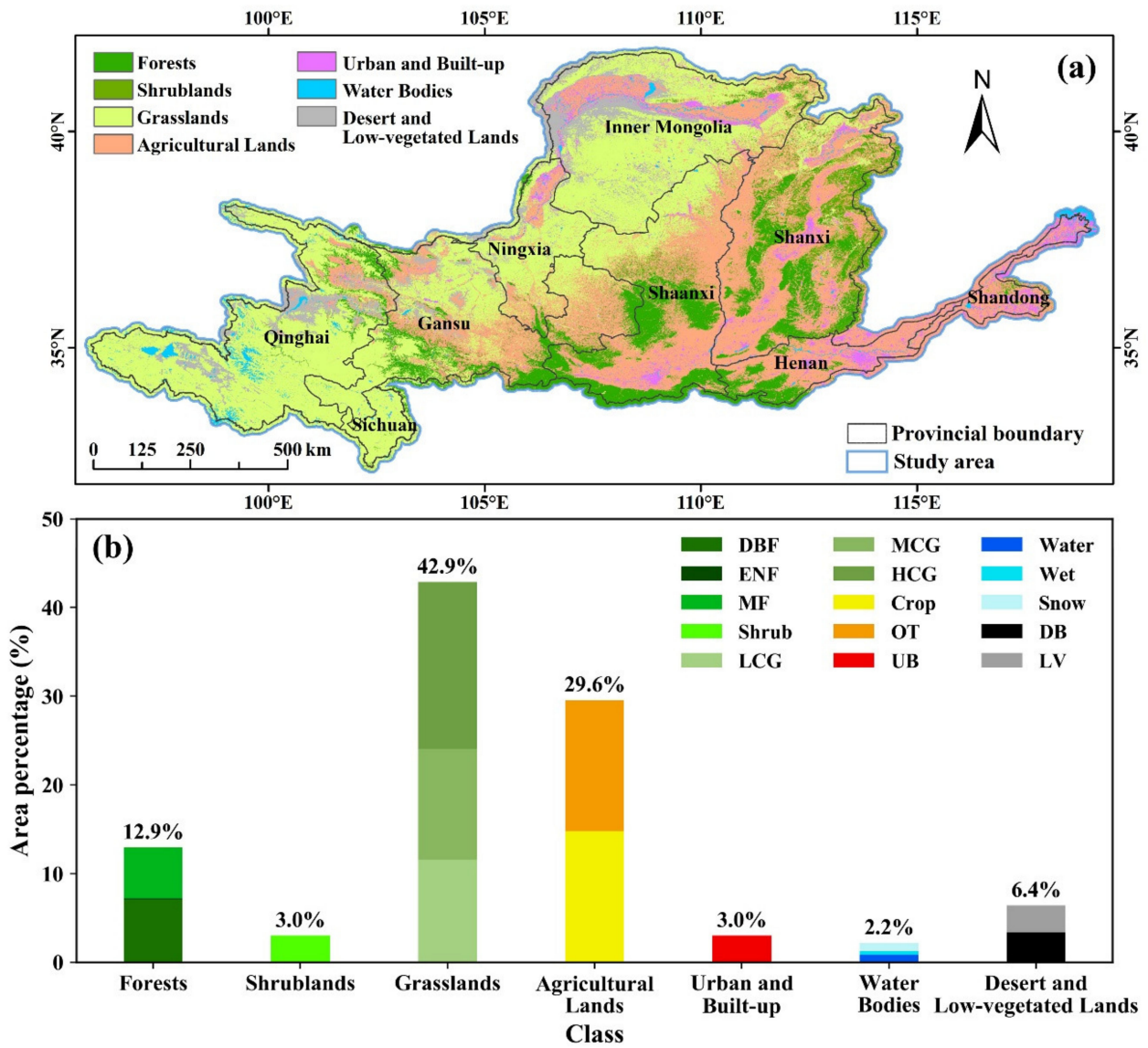


Figure 3. (a) Spatial distribution of land use/cover of the Yellow River basin in 2018 and (b) the average area percentage of each land use/cover class during the study time period. The abbreviation of each class in Figure 3b can be found in Table 2.

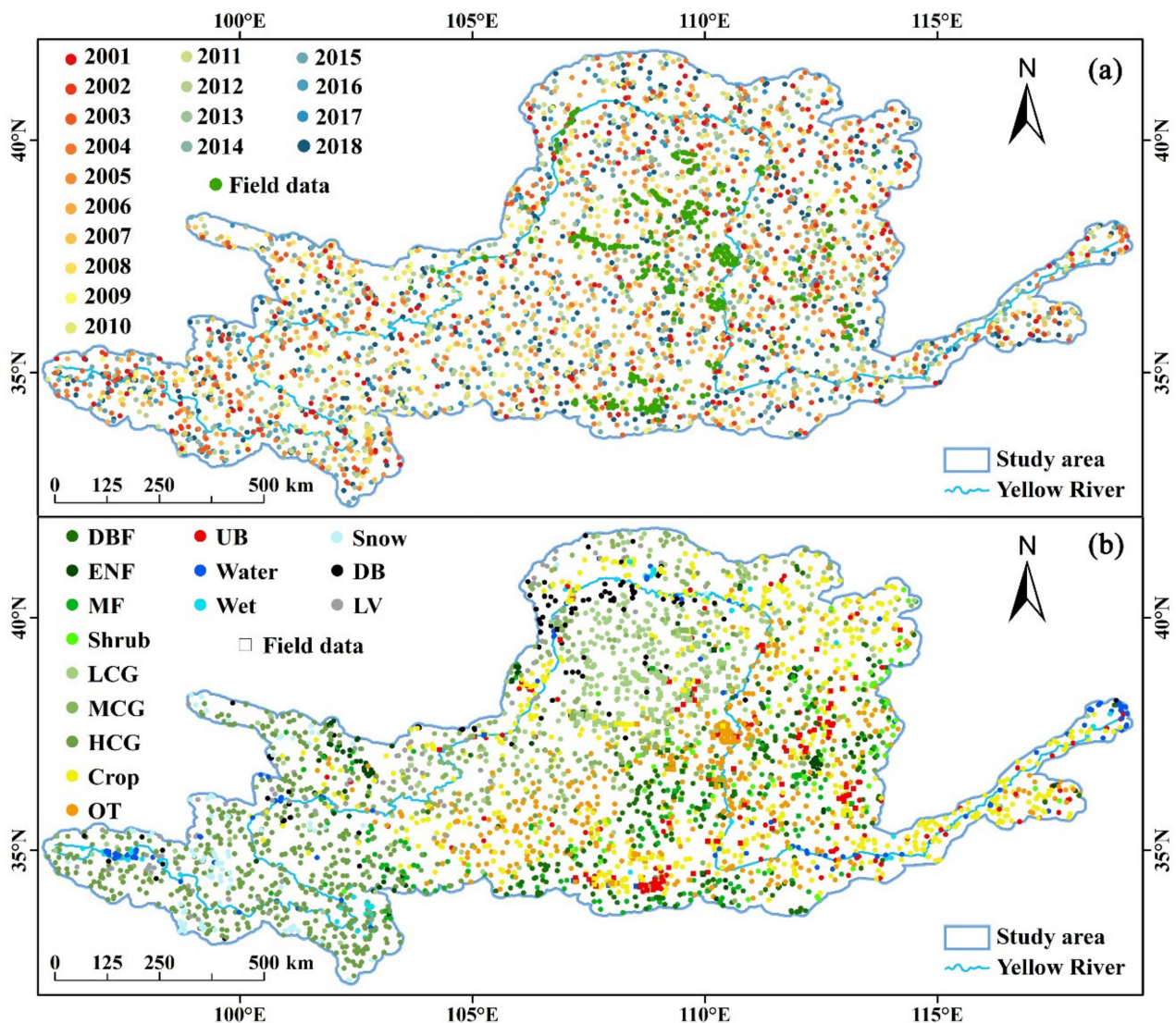


Figure 4. (a) The year and geographical distribution of validation points sets. (b) The class and geographical distribution of validation points sets. Including 3456 random validation points on Google Earth and 640 ground points from the field survey.

When comparing with seven other data products, it was found that our land use/cover data has high consistency with GlobeLand30 and CGLS-LC100 in terms of spatial details and land area statistics (Figures S10 and S11). Both of them can distinguish water bodies, urban and built-up, and agricultural lands better with the finer spatial resolution. Compared to other data products, our land use/cover map can better distinguish between the croplands in the flat areas and the OT distributed on the sloped land where the land is more affected by human activities. Furthermore, the FROM-GLC (2010) has obvious edge effects between Landsat scenes and scenes and caterpillar track damage, which be repaired in this study (Figure S10). The areas of shrublands, urban and built-up, water bodies, and desert and low-vegetated lands in all other datasets were not much different from this study. However, there were obvious differences in the total area of agricultural lands (croplands and OT) and grasslands, which may be caused by differences in the class definition in the different classification schemes. Such as, MCD12Q1-V6 has larger grasslands and smaller agricultural lands, which is contrary to that of GlobCover. Then, we collected statistical data on the available cropland area of 292 counties within the study area from 1990 to 2014 and compared the area of cropland in six land use/cover products for different periods (Figure S12). The results showed that the croplands in our land use/cover data displayed

a good consistency with the statistical data, indicated by a relatively larger coefficient of determination (R^2) and smaller root mean square errors (RMSE). In general, the annual land use/cover map series of the YR basin from 1986 to 2018 with high accuracies have a reasonable consistency with other land use/cover products and statistics, which can be used to explore regional land use/cover and its changes patterns.

Table 3. Confusion matrix of 3456 independent stratified random sampling validation points set from 2001 to 2018. UA denotes user's accuracy, PA denotes producer's accuracy, F1-score is the weighted harmonic mean of PA and UA, and bold numbers represent correctly classified ones.

		Prediction															
Class	DBF	ENF	MF	Shrub	LCG	MCG	HCG	Crop	OT	UB	Water	Wet	Snow	DB	LV	PA	
Reference	DBF	160	0	1	6	1	3	0	2	25	3	1	0	0	0	79%	
	ENF	1	80	1	2	1	0	0	0	1	0	0	0	0	0	93%	
	MF	1	1	130	1	1	0	0	1	0	0	0	0	0	0	96%	
	Shrub	2	0	1	67	5	0	2	0	4	1	0	0	0	0	82%	
	LCG	4	0	3	0	205	14	12	4	10	6	1	1	4	1	0	77%
	MCG	0	0	2	0	2	225	13	6	12	2	1	0	0	0	1	85%
	HCG	2	2	2	0	2	2	430	5	11	0	0	4	2	0	0	93%
	Crop	8	0	5	4	51	31	5	332	30	25	4	10	0	4	2	65%
	OT	9	2	8	4	8	42	0	15	269	1	0	3	0	0	4	74%
	UB	0	0	0	0	8	5	0	6	10	44	0	0	0	0	1	59%
	Water	0	0	0	0	0	0	0	0	1	3	77	18	1	1	1	75%
	Wet	0	0	0	0	0	0	1	0	0	0	0	46	0	0	0	98%
	Snow	0	0	0	0	0	0	7	1	0	0	0	2	71	1	2	85%
	DB	0	0	0	0	5	2	3	1	1	0	1	1	3	76	0	82%
	LV	0	0	1	0	0	0	3	1	0	0	0	0	4	2	73	87%
	UA	86%	94%	84%	80%	71%	69%	90%	89%	72%	52%	91%	54%	84%	89%	87%	80%
F1-score	0.82	0.94	0.90	0.81	0.74	0.77	0.92	0.75	0.73	0.55	0.82	0.70	0.84	0.85	0.87		
Support	202	86	135	82	265	264	462	511	365	74	102	47	84	93	84		

3.2. Land Use/Cover Change Patterns

During the study period, the land use/cover of the YR basin changed substantially in terms of both spatial patterns and area. The geographical distribution of change in area ratio and the land use/cover transition matrix were computed to detect the transition of different land use/cover classes (Figure 5 and Table 4). The land use/cover transition matrix showed that land use/cover changes mainly occurred in the transition from forests, grasslands, and croplands to the class of OT, accounting for 19.77% of the total change area (69,586 km²). Another obvious case was the transition of croplands to UB, accounting for 5.74% of the total change (20,200 km²). The areas where UB increased and croplands decreased were mainly distributed along the middle and lower reaches of the YR. Obvious decreases in water bodies were found in the YR source region. Area of the desert and low-vegetated lands have also decreased in the northwestern YR basin. More obviously, the area of OT increased significantly in the hilly areas on the Loess Plateau. Five LUCC patterns were clustered, manifesting different characteristics of change (Figure 5i), which are as follows: (1) no change or little change, (2) cropland loss and urban expansion, (3) grassland restoration, (4) increase in orchard and terrace, and (5) increase in forest.

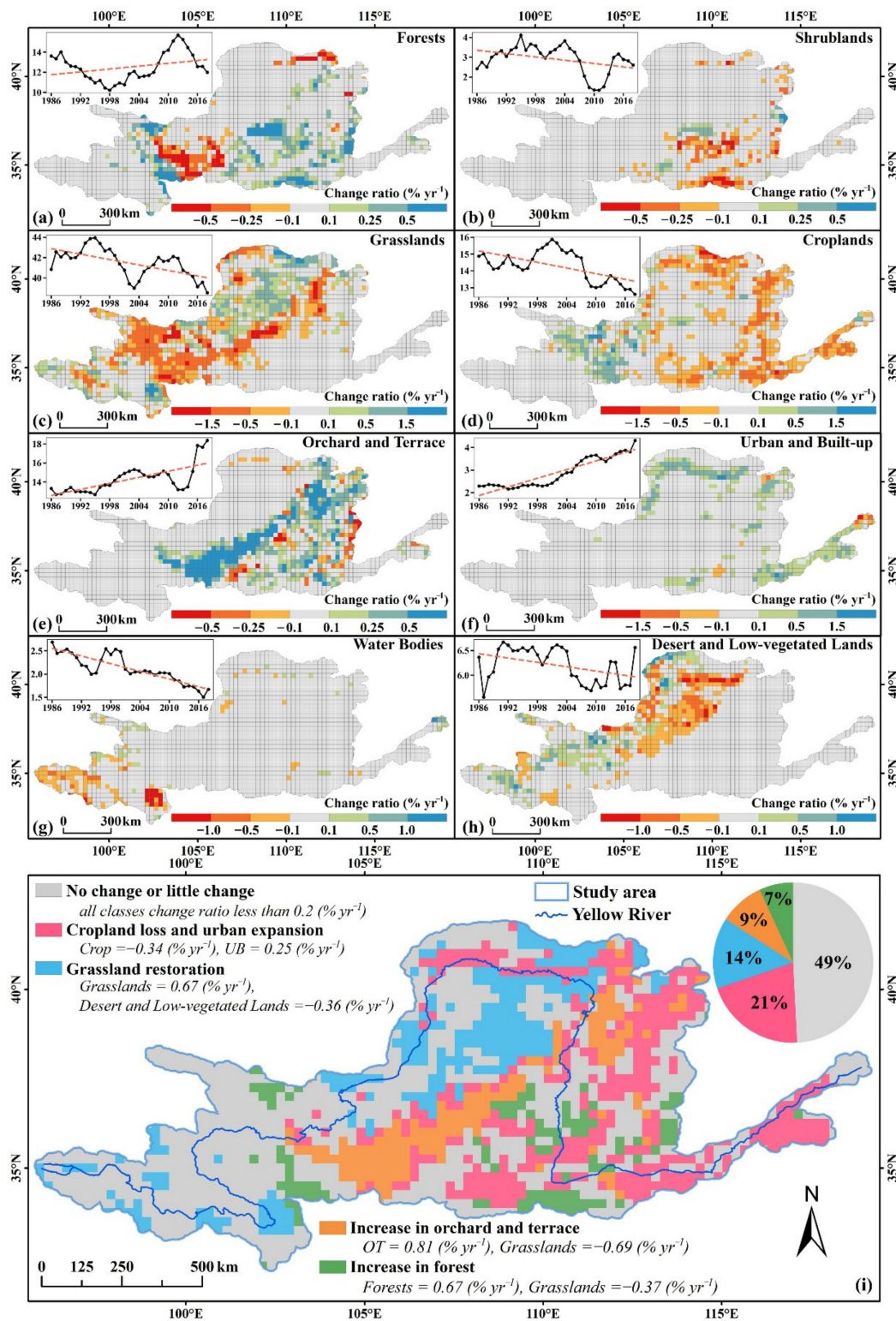


Figure 5. Geographical distribution of the YR basin with significant ($p < 0.05$) change in area ratio per year during 1986–2018 for each class: (a) forests, (b) shrublands, (c) grasslands, (d) croplands, (e) orchard and terrace, (f) urban and built-up, (g) water bodies, and (h) desert and low-vegetated lands. Grey grids show the areas with a statistically insignificant change slope or change ratio below 0.1 \% yr^{-1} (-0.1 to 0.1). Insets in each graph show the annual area (10^4 km^2) of each class from 1986 to 2018. (i) Geographical distribution of five LUCC patterns in the YR basin. Italic indicates the average change rate of the corresponding pattern.

Table 4. Land use/cover transition matrix of the study area. Cell values represent the area (10⁴ km²) of land use/cover transitions from 1986 to 2018, and bold numbers represent correctly classified ones

Class	2018																
	DBF	ENF	MF	Shrub	LCG	MCG	HCG	Crop	OT	UB	Water	Wet	Snow	DB	LV	Total	
1986	DBF	3.54	0.01	1.18	1.04	0.05	0.44	0.17	2.38	0.01					0.04	8.87	
	ENF	0.01	0.03	0.11	0.02											0.17	
	MF	0.85	0.05	2.59	0.32	0.01	0.01	0.16	0.26	0.28					0.06	4.58	
	Shrub	0.57		0.54	0.61	0.01	0.03		0.67							2.43	
	LCG	0.11		0.06	0.04	7.54	1.39	0.41	1.43	0.17	0.01			0.38	0.15	11.68	
	MCG	0.06		0.02	0.01	0.96	6.48	0.71	1.35	0.16	0.01			0.36	0.79	10.91	
	HCG	0.01		0.81		0.04	0.02	15.93	0.29		0.02	0.01	0.13	0.17	0.83	18.26	
	Crop	0.09		0.07	0.02	0.66	0.72	0.07	9.32	1.52	2.02	0.06	0.09		0.14	0.10	14.88
	OT	0.70		0.53	0.55	0.39	0.23		0.33	10.40	0.15	0.02			0.03	13.33	
	UB			0.01		0.14	0.07		0.58	0.23	1.26	0.14	0.02		0.03	0.03	2.52
	Water					0.01	0.01	0.04	0.16	0.02	0.19	0.42	0.05		0.01	0.02	0.94
	Wet					0.02		0.49	0.02	0.01	0.03	0.03	0.08	0.03	0.02	0.07	0.80
	Snow					0.01		0.48						0.44		0.01	0.94
	DB					0.77	0.23	0.18	0.25		0.23	0.02	0.02	0.06	1.84	0.41	4.01
	LV			0.03		0.15	0.45	0.37	0.09	0.07	0.07	0.01	0.01	0.01	0.11	0.99	2.35
	Total	5.94	0.09	5.96	2.61	10.75	10.09	17.71	12.60	18.38	4.31	0.73	0.28	0.66	3.05	3.51	96.67

3.3. The Transition from Multiple Land Use/Cover Classes to Orchard and Terrace

Generally, OT has increased by 50,512 km² (38%) from 1986 to 2018, as a result of a net gain of 79,710 km² balanced by a loss of 29,198 km². We further mapped the spatiotemporal distribution of the transition from forests, grasslands, and croplands to OT with more details in Figure 6a and Figure S13. It was found that the transition from forests to OT mainly occurred in the marginal area of primary forests, indicating that human activities gradually intruded into natural forests. By contrast, the transition from grasslands to OT mainly occurred in the northern Shaanxi and eastern Gansu province, while the transition from croplands to OT mainly occurred on the slopes at the junction of plains and mountains. We further explored the transition sources and destination of the OT during the past 33 years (Figure 6b). Again, accompanied by mutual transition with other land use/cover classes, the area of OT was gradually increasing, with substantial gains in two remarked periods of 1995–2003 and 2013–2018. From 1995 to 2003, 18,823 km² of grasslands and 8518 km² of croplands were converted to OT, whereas the substantial increase in OT was the transition from forests from 2013 to 2018 (29,635 km²).

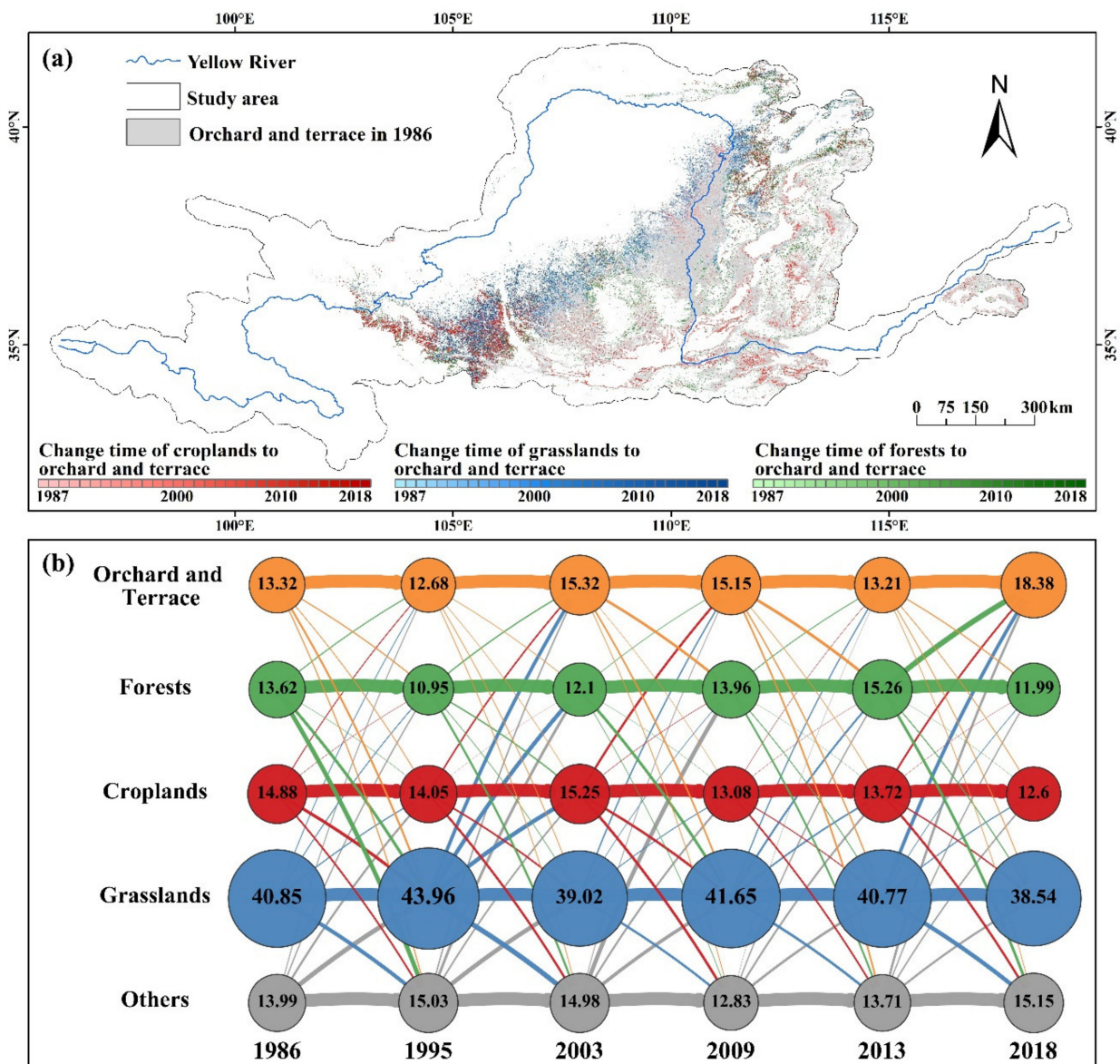


Figure 6. The transition of multiple land use/cover classes to orchard and terrace (OT). (a) Spatiotemporal distribution of the transition of forests, grasslands, and croplands to OT. (b) Land use/cover transition network of all the pixels in the study area for different periods. The numbers within the cycles in Figure 6b are the area (10^4 km^2) of each class in the corresponding year. The lines represent the amount of land use/cover transition area and their colors are the same as the source of transition.

4. Discussion

4.1. Limitations

According to the accuracy assessment, it can be seen that this annual land use/cover products of the YR basin are reliable and accurate, and that the annual land use/cover mapping framework is effective. However, there are still some deficiencies in this mapping framework.

Our land use/cover products were first limited by Landsat images quality and quantity, which was influenced by satellite sensors and clouds [60]. The source region of the YR with high-altitude is a representative example, where is covered by heavy clouds. Besides, due to the low temporal resolution (i.e., 16 days) and known issues of Landsat 7, the missing data was inevitable to be filled. All of which will reduce the accuracy of image classification and LUCC detection. On the other hand, the annual maps were composited

from scenes at different times in the chosen time window and the spectral differences of different time-series Landsat images will lead to some uncertainties. Although we have performed time-consistent post-processing of the classification results, the interannual fluctuations in data cannot be completely avoided. In addition, with rapid urbanization and industrialization, coupled with specific climatic conditions and topographic features, severe fog-haze has appeared in some cities in China [61], which will also affect the accuracy of land use/cover classification [62]. A typical example was a distinction between UB and croplands distributed around Taiyuan, which is located between Taihang Mountain and Lvliang Mountain. The geographic features of mountainous regions are not conducive to the dissipation of fog-haze, thus leading to an overestimation of the UB area.

Secondly, the training sample data used were manually drawn on GEE referring to Google Earth images and Landsat annual composite images. The image of quality is not high and there are few high-resolution reference images for judgment, especially in earlier years (before 2000). The error in artificial judgment, imperfections in the sample size, and mixed pixels may induce uncertainties in the classification [63]. Besides, in data validation, limited by the error in manual judgment and the uneven distribution of verification points in time, there are also certain uncertainties in the assessment of land use/cover maps. This uncertainty will further cause errors and some uncertain effects in the estimate and analysis of the area of each class in the subsequent analysis [58,64].

Thirdly, the classification scheme of our study integrated land use/cover. Natural forests and planted ecological forests were classified as forests while the economic forest was classified as orchard and terrace. In the OT class, there were arbors, such as apple and apricot, and shrubs such as jujube and grapes. In the early stages of plant growth, the biophysical properties of artificially planted ecological and economic trees are quite difficult to be captured by remote sensing observations, which caused some misclassifications among OT, forests, and shrublands.

In recent years, many land use/cover mapping methods with sophisticated algorithms and data processing have been developed, such as seasonal composite image classification [65], multi-temporal data classification [66], Object-Oriented classification [67], and Maximum Likelihood and Spectral Angle Mapper classification [68] (See more methods in Table S6). Here, the processing of the annual land use/cover map was completely based on the powerful cloud storage and cloud computing capabilities of the GEE platform with free and direct access satellite images and classification methods (CART), which can mitigate the pressure of local data storage and data processing. Although the above limitations and methodological deficiencies, our workflow and analysis strategy can flexibly and effectively be used to map the land use/cover dynamics in such hot spot basins.

4.2. Land Use/Cover Dynamics and Potential Causes

Our mapping can reveal the important role of forest management in altering land use/cover in the region over the 33 years. Namely, forest firstly showed a gradual decrease from 1986 to 1998, then increased until 2012. After 2012, it went down year by year (Figure 5a and Figure S14). This may be related to the following reasons. Firstly, as stated earlier, the Chinese government has initiated the GFG program since 1999 over the study area, the Loess Plateau, in particular. The large-scale afforestation has led to a rapid increase in forests during the period 1999–2012, which was also consolidated by many previous studies in this area [17,69]. The forest loss after 2012 was mainly concentrated in the continuous poverty-stricken mountainous areas, such as Liupan Mountain and Lvliang Mountain. In these regions, once the compensation from the government is inadequate or will end, farmers live in these mountainous and hilly areas may again convert afforestation on their lands back to agricultural land [22,70–72]. On the other hand, the spatial pattern of land use/cover change and transition network have indicated that most of the loss forest have converted to OT (Figure S14a), which reflect the change in the policy of the GFG program. Specifically, compared to the first round of the GFG program (1990–2010), to lift groups of destitute communities out of poverty and promote rural economic development, the second

round of this program (initiated in 2014) encouraged farmers to develop economic trees as a priority (not ecological forests) by enhancing its financial compensation (increased by 300 yuan per 667 m²). This may have resulted in a forest loss, which was further corroborated by the rapid increase in OT after 2014 (Figures 5a and 6b). The same reasons can be explained for the changes in grassland. The analysis results show that the forests and grassland in the study area have been lost due to changes in land use under the strong human activities. The physical and chemical properties of these land have also changed [73]. As the restored ecological forest and restored economic forest have different ecosystem services from natural forest [74], some ecological and environmental problems may arise. Therefore, long-term and continuous monitoring of the LUCC is critical for determining the effects of the existing GFG program, which also reminds us that we need to continue to protect and consolidate the results of the GFG program. While improving the quality and efficiency of agriculture and guaranteeing farmers' income, we also need to further strengthen the protection of natural and ecological forests, improve land use efficiency, and realize the scientific and sustainable use of land resources.

Besides the transition from forests, grassland and cropland also contributed to the increase in OT (Figure 6). Previous studies have shown that a large number of fruits have been planted in the Loess Plateau during recent years, such as apple, jujube, and peach. Statistics also showed that the fruit area and fruit production in the plateau increased by 1-fold and 3-fold, respectively, from 1998 to 2016. This land use/cover transition indicated the agricultural economic structure of YR had changed. It was confirmed by a recent study which has stated that the ratio of fruit production to the total crops on the Loess Plateau increased from 14% to 23%, while grain crops decreased from 44% to 37% over the period 2000–2015 [75]. These economic trees not only increased the greenness but also raised the income [69,76]. YR will achieve a win-win scenario balancing the smooth implementation of the government's environmental protection policy and increase in farmers' income. For example, a study in a small watershed on the Loess Plateau has shown that fruit sales as a percentage of total income increased dramatically by 59%, which may be existed in similar rural areas [77]. The massive increase in OT suggested that YR progress towards sustainable development goals for livelihood security, economic growth, and ecosystem conservation. In fact, China has made great efforts for achieving global Sustainable Development Goals (SDGs) via a diverse range of policy instruments [22,78]. A recent study has shown that investment in the 16 major sustainability programs for the land-system in China was far exceeded other globally important national sustainability programs [22,79]. These programs have substantially improved agricultural production efficiency, natural environment, and the quality of life in rural areas through agricultural production and cultivated land protection, forest ecosystem protection, and grassland restoration, which promotes the sustainable development of human and natural systems and reflects a great achievement of policy and governance of China. The land use/cover transition of our findings was just a specific embodiment of one aspect. All of which reflected the rapid land use/cover dynamics with intense human activities in a short time on the YR basin, highlighting the importance of annual maps of land use/cover for understanding the interaction between human and natural systems.

Our findings showed that cropland has experienced a slightly decreasing trend from 1986 to 1995, followed by an obviously increasing trend from 1996 to 2000 (Figure 5d and Figure S15). After that, this increasing trend has been markedly reversed. These temporal changes were also confirmed by the statistical data (Figure S15d). This may stem from the following fact. Since the economic reform was implemented in 1978, China has witnessed a large-scale urban expansion and dramatic decline in croplands. Coupled with the serious environmental issues from land desertification and soil erosion, the arable area decreased slowly. Since the 1990s, due to the rapid population growth and the improvement of living standards, the demand for food consumption has increased but arable land resources were limited. To curb the continuous reduction of arable land and ensure food security, the Chinese government proposed a series of cropland protection policies (e.g., the Arable

Land Requisition-Compensation Balance policy) in the late 1990s [80]. Driven by local governments and economic interests, a large number of grasslands and unused land have been reclaimed as cropland [81], especially in Shanxi, Inner Mongolia, Qinghai, Ningxia, and Gansu province (Figure S15b,d). The continuous and widespread decrease of cropland after 1999 was mainly because of the implementation of the well-known GFG program and the accelerating urban expansion (Figure 5f). The rapid development of the socio-economy has promoted the continuous improvement of the level of urbanization and industrialization in the YR basin. Unfortunately, the expansion of these cities largely encroached upon cropland (Figure S16). The continued expansion of urbanization has posed great challenges to guaranteeing local and regional food security [14,82]. Therefore, to meet the food demand by the ever-growing population, the increase in the harvested area through agricultural intensification with better land management practices should be considered, while avoiding over-farming and agricultural pollution, which is the prerequisite for sustainable development in this region.

Spatially contiguous hotspots of gain in grasslands and decrease of the desert and low-vegetated lands were found in the Mu Us Desert, confirming the effectiveness of the large-scale vegetation restoration induced by China's national policies for the ecosystem, such as the NFC program and the GFG program. Our finding that the area of DB has decreased over the study areas from 1986 to 2018 also suggests a net increase in vegetation cover. However, some regions on the YR basin still faced land degradation concerns. The headwaters of the YR basin, which is called the water tower of this basin, contributed 35% of total water resources in the basin [83]. The total area of lakes and swamps of this region is approximate 2000 km². Our land use/cover record witnessed severe water body shrinkage (Figure 5g), most of which degraded into low-vegetated lands (Figure 5h) or high coverage grasslands (Figure 5c). The decline of the water body area will potentially shift this fragile ecosystem to an irreversible state [84]. This shows that the land system and water security of the Yellow River basin are still under threat.

5. Conclusions

Accurate and long-term land use/cover data is critical for land conservation and management in the YR basin. We analyzed all the available Landsat imagery (17,080 images) using the GEE platform and CART algorithm to produce a set of annual land use/cover data at 90 m resolution spanning the 33 years from 1986 to 2018. The classification scheme is adjusted based on the capability of the data used and the characteristics of the YR basin. Accuracy was improved by multi-source incorporating feature sets, Landsat data filtering and anomalous data repair methods, feature variable selection, and result optimization strategy. The assessment based on 640 validation points collected from field surveys and 3456 independent stratified random sampling validation points collected in Google Earth indicated that the overall accuracy of these maps is 78.3% and 80.0%, respectively.

Results demonstrated that land use/cover of the YR basin presents complicated spatial and temporal transitions during the entire study period, which was mainly driven by political, social, and economic factors. Five LUCC patterns were clustered, manifesting different characteristics of change, which are as follows: no change or little change, cropland loss and urban expansion, grassland restoration, increase in orchard and terrace, and increase in forest. The land use/cover transition matrix analysis showed that the primary LUCC was mainly due to an increase of orchard and terrace resulted from forests, grasslands, and croplands (19.8% of all changes area) and the urban expansion with a loss of cropland (5.7% of all changes area). Substantial gains in orchard and terrace in the period of 1995–2003 were mainly converted from grasslands and croplands, whereas in 2013–2018 is mostly from forests. These economic trees planted on orchard and terrace not only increased the greenness, but also raised the income, suggesting that YR progress towards the sustainable development goals for livelihood security, economic growth, and ecological protection. However, the conversion of ecological forests to economic forests may cause some ecological and environmental problems, which also reminds us that we

need to continue to protect the natural and ecological land, improve land use efficiency, and realize the scientific and sustainable use of land resources.

The mapped LUCC captured the modification of Earth's terrestrial surface on this strong coupled human-nature system and provide insights into the impacts of environmental policy and socio-economic activities on land. The data-driven approach we used here, which is based on high-resolution satellite data and physiography data built by landforms and lithology, can flexibly and effectively be used to model the land use/cover dynamics in other hotspot basins. The land use/cover dynamics and their change patterns provide important information in facilitating the formulation of effective strategies for sustainable and high-quality development in the YR basin and similar regions.

Supplementary Materials: The following are available online at <https://www.mdpi.com/article/10.3390/rs13071299/s1>, Figure S1: Geographical distribution of Landsat scenes used; Figure S2: (a) Christmas tree anomaly. (b) Caterpillar tracks run throughout the whole image scene. (c) Statistically monitor the annulus area to identify the scene which has caterpillar tracks. The purpose of using annulus instead of rectangular bounds of image scene is to save GEE user memory. (d) The gap filling of missing data and Landsat 7 gaps; Figure S3: Comparison of 6 composite methods image effects achieved in GEE on two areas; Figure S4: The distribution of training sample polygons in time and class; Figure S5: Moving the sliding window to adjust temporal consistency and the accuracy is calculated by reference samples in each year; Figure S6: The geographical distribution of ground points for validation. These points were collected during the field survey in 2015, 2017, and 2018 within the Yellow River basin. Insets are the illustration of some points; Figure S7: Training accuracy of classifiers and the number of Landsat scenes used in each year. The accuracy range is determined by the maximum and minimum value of 10 times classifications in each year; Figure S8: Average of the count of unique values in 10 classifications for each pixel each year for 33 years. The classifiers are more stable in areas with smaller values; Figure S9: Normalized confusion matrix of 3456 independent stratified random sampling validation points set from 2001 to 2018; Figure S10: Comparison of different land use/cover datasets within a region in the middle reaches of the Yellow River in 2010 and 2015. The data of this study divides agricultural lands into croplands and orchard and terrace classes; Figure S11: The difference in area between other land use/cover products and this study in the first-degree classes (this study—other product); Figure S12: Comparisons between the estimated croplands areas in each product and those obtained from the statistical dataset in different time periods; Figure S13: Examples of the transition of forests (a), grasslands (b), and croplands (c) to orchard and terrace (OT) on Google Earth images, respectively; Figure S14: Change in forests from 1986 to 2018. (a) Land use/cover transition network of all the pixels in the study area for different periods. The numbers within the cycles in the figure is the area (104 km²) of each class in the corresponding year. Geographical distribution of the change of forests area ratio during (b) 1986–1998, (c) 1998–2012, and (d) 2012–2018 in the Yellow River basin. The change in area ratio was obtained in each grid (0.5°); Figure S15: Change in croplands from 1986 to 2018. (a) Land use/cover transition network of all the pixels in the study area for different periods. The numbers within the cycles in the figure is the area (104 km²) of each class in the corresponding year. Geographical distribution of the change of croplands area ratio during (b) 1986–2001 and (c) 2001–2018 in the Yellow River basin. The change in area ratio was obtained in each grid (0.5°). (d) The change of croplands area on Loess Plateau from 1990 to 2014 which got from statistical data. The 1980S represents the average value from 1980 to 1989; Figure S16: Geographical distribution of croplands to urban and built-up in six major cities of Yellow River basin: (a) Zhengzhou, (b) Xi'an, (c) Taiyuan, (d) Lanzhou, (e) Hohhot, and (f) Xining; Table S1: Land cover and land use data used in related studies on the Yellow River basin. The Cbers denotes China-Brazil Earth Resources Satellite; Table S2: The accuracy of different band combinations. The values in the table represent the F1-score (the weighted harmonic mean of the producer's and user's accuracy) of each classifier in each class. Orange represents the corresponding classifier is better than the classifier with only using Landsat 6 spectral bands and blue represents the opposite case. The bands marked by * are the band combination for final classification. Aspect, landforms, Continuous Heat-Insolation Load Index (CHILI), and Multi-Scale Topographic Position Index (mTPI) are calculated from SRTM data. Enhanced Vegetation Index (EVI), Green Chlorophyll Vegetation Index (GCVI), and Atmospherically Resistant Vegetation Index (ARVI) are calculated from Landsat bands; Table S3: Confusion matrix of validation for test classifier in 2010. The overall

accuracy is 90% and the Kappa coefficient is 0.89. UA denotes user's accuracy, PA denotes producer's accuracy, and bold numbers represent correctly classified ones; Table S4: Test results for different classification methods; Table S5 Land use/cover datasets for comparison; Table S6: List of related land use/cover mapping articles.

Author Contributions: Conceptualization, W.L. and Y.L.; methodology, Q.J.; software, Q.J.; validation, Q.J., S.L., P.Y., and Z.L.; formal analysis, Q.J., W.Z., and W.L.; investigation, Q.J.; data curation, Q.J., W.Z., and Z.L.; writing—original draft preparation, Q.J. and W.Z.; writing—review and editing, W.L., J.Y., C.Y., Y.L., B.F., and Z.J.; visualization, Q.J. and Z.L.; supervision, W.L.; project administration, Y.L.; funding acquisition, W.L., J.Y. and Y.L. All authors have read and agreed to the published version of the manuscript.

Funding: This research was funded by the National Key Research and Development Program of China (2016YFC0501601), the National Natural Science Foundation of China (41771118,41501093), and the Fundamental Research Funds for the Central Universities, Shaanxi Normal University (GK201802004, GK202003060).

Institutional Review Board Statement: Not applicable.

Informed Consent Statement: Not applicable.

Data Availability Statement: The data presented in this study are available in the Supplementary Materials, or please contact the author of this article.

Acknowledgments: Acknowledgement for the statistical data support from “National Earth System Science Data Center, National Science & Technology Infrastructure of China. (<http://www.geodata.cn>)”. The authors thank Yingjie Li from Michigan State University for his insightful comments and suggestions for this paper.

Conflicts of Interest: The authors declare no conflict of interest.

References

- Lambin, E.F.; Meyfroidt, P. Global land use change, economic globalization, and the looming land scarcity. *Proc. Natl. Acad. Sci. USA* **2011**, *108*, 3465–3472. [[CrossRef](#)]
- Liu, H.; Gong, P.; Wang, J.; Clinton, N.; Bai, Y.; Liang, S. Annual dynamics of global land cover and its long-term changes from 1982 to 2015. *Earth Syst. Sci. Data* **2020**, *12*, 1217–1243. [[CrossRef](#)]
- Turner, B.L., II; Lambin, E.F.; Reenberg, A. The emergence of land change science for global environmental change and sustainability. *Proc. Natl. Acad. Sci. USA* **2007**, *104*, 20666–20671. [[CrossRef](#)] [[PubMed](#)]
- Song, X.P.; Hansen, M.C.; Stehman, S.V.; Potapov, P.V.; Tyukavina, A.; Vermote, E.F.; Townshend, J.R. Global land change from 1982 to 2016. *Nature* **2018**, *560*, 639–643. [[CrossRef](#)]
- Duveiller, G.; Hooker, J.; Cescatti, A. The mark of vegetation change on Earth's surface energy balance. *Nat. Commun.* **2018**, *9*, 679. [[CrossRef](#)] [[PubMed](#)]
- Young, N.L.; Lemieux, J.M.; Delottier, H.; Fortier, R.; Fortier, P. A Conceptual Model for Anticipating the Impact of Landscape Evolution on Groundwater Recharge in Degrading Permafrost Environments. *Geophys. Res. Lett.* **2020**, *47*, e2020GL087695. [[CrossRef](#)]
- Yue, C.; Ciaia, P.; Houghton, R.A.; Nassikas, A.A. Contribution of land use to the interannual variability of the land carbon cycle. *Nat. Commun.* **2020**, *11*, 3170. [[CrossRef](#)]
- Jones, K.R.; Venter, O.; Fuller, R.A.; Allan, J.R.; Maxwell, S.L.; Negret, P.J.; Watson, J.E.M. One-third of global protected land is under intense human pressure. *Science* **2018**, *360*, 788–791. [[CrossRef](#)]
- Marques, A.; Martins, I.S.; Kastner, T.; Plutzer, C.; Theurl, M.C.; Eisenmenger, N.; Huijbregts, M.A.J.; Wood, R.; Stadler, K.; Bruckner, M.; et al. Increasing impacts of land use on biodiversity and carbon sequestration driven by population and economic growth. *Nat. Ecol. Evol.* **2019**, *3*, 628–637. [[CrossRef](#)]
- Tilman, D.; Socolow, R.; Foley, J.A.; Hill, J.; Larson, E.; Lynd, L.; Pacala, S.; Reilly, J.; Searchinger, T.; Somerville, C. Beneficial biofuels—the food, energy, and environment trilemma. *Science* **2009**, *325*, 270–271. [[CrossRef](#)]
- Foley, J.A.; Defries, R.; Asner, G.P.; Barford, C.; Bonan, G.; Carpenter, S.R.; Chapin, F.S.; Coe, M.T.; Daily, G.C.; Gibbs, H.K.; et al. Global consequences of land use. *Science* **2005**, *309*, 570–574. [[CrossRef](#)] [[PubMed](#)]
- Paul, J.; Mas, E. The Emergence of China and India in the Global Market. *J. East-West Bus.* **2016**, *22*, 28–50. [[CrossRef](#)]
- Chen, C.; Park, T.; Wang, X.; Piao, S.; Xu, B.; Chaturvedi, R.K.; Fuchs, R.; Brovkin, V.; Ciaia, P.; Fensholt, R.; et al. China and India lead in greening of the world through land-use management. *Nat. Sustain.* **2019**, *2*, 122–129. [[CrossRef](#)] [[PubMed](#)]
- Chen, Y.P.; Wang, K.B.; Lin, Y.S.; Shi, W.Y.; Song, Y.; He, X.H. Balancing green and grain trade. *Nat. Geosci.* **2015**, *8*, 739–741. [[CrossRef](#)]

15. Lu, Y.; Zhang, L.; Feng, X.; Zeng, Y.; Fu, B.; Yao, X.; Li, J.; Wu, B. Recent ecological transitions in China: Greening, browning, and influential factors. *Sci. Rep.* **2015**, *5*, 8732. [[CrossRef](#)] [[PubMed](#)]
16. Wang, F.; Mu, X.; Li, R.; Fleskens, L.; Stringer, L.C.; Ritsema, C.J. Co-evolution of soil and water conservation policy and human-environment linkages in the Yellow River Basin since 1949. *Sci. Total Environ.* **2015**, *508*, 166–177. [[CrossRef](#)]
17. Fu, B.J.; Wang, S.; Liu, Y.; Liu, J.B.; Liang, W.; Miao, C.Y. Hydrogeomorphic Ecosystem Responses to Natural and Anthropogenic Changes in the Loess Plateau of China. *Annu. Rev. Earth Planet. Sci.* **2017**, *45*, 223–243. [[CrossRef](#)]
18. Zhao, J.; Yang, Y.; Zhao, Q.; Zhao, Z. Effects of ecological restoration projects on changes in land cover: A case study on the Loess Plateau in China. *Sci. Rep.* **2017**, *7*, 44496. [[CrossRef](#)]
19. Feng, X.; Fu, B.; Piao, S.; Wang, S.; Ciais, P.; Zeng, Z.; Lü, Y.; Zeng, Y.; Li, Y.; Jiang, X.; et al. Revegetation in China's Loess Plateau is approaching sustainable water resource limits. *Nat. Clim. Chang.* **2016**, *6*, 1019–1022. [[CrossRef](#)]
20. Liang, W.; Fu, B.; Wang, S.; Zhang, W.; Jin, Z.; Feng, X.; Yan, J.; Liu, Y.; Zhou, S. Quantification of the ecosystem carrying capacity on China's Loess Plateau. *Ecol. Indic.* **2019**, *101*, 192–202. [[CrossRef](#)]
21. Liang, W.; Bai, D.; Wang, F.Y.; Fu, B.J.; Yan, J.P.; Wang, S.; Yang, Y.T.; Long, D.; Feng, M.Q. Quantifying the impacts of climate change and ecological restoration on streamflow changes based on a Budyko hydrological model in China's Loess Plateau. *Water Resour. Res.* **2015**, *51*, 6500–6519. [[CrossRef](#)]
22. Bryan, B.A.; Gao, L.; Ye, Y.; Sun, X.; Connor, J.D.; Crossman, N.D.; Stafford-Smith, M.; Wu, J.; He, C.; Yu, D.; et al. China's response to a national land-system sustainability emergency. *Nature* **2018**, *559*, 193–204. [[CrossRef](#)]
23. Song, Y.; Xue, D.; Dai, L.; Wang, P.; Huang, X.; Xia, S. Land cover change and eco-environmental quality response of different geomorphic units on the Chinese Loess Plateau. *J. Arid Land* **2019**, *12*, 29–43. [[CrossRef](#)]
24. Theobald, D.M.; Harrison-Atlas, D.; Monahan, W.B.; Albano, C.M. Ecologically-Relevant Maps of Landforms and Physiographic Diversity for Climate Adaptation Planning. *PLoS ONE* **2015**, *10*, e0143619. [[CrossRef](#)] [[PubMed](#)]
25. Delang, C.O.; Yuan, Z. *China's Grain for Green Program: A Review of the Largest Ecological Restoration and Rural Development Program in the World*; Springer International Publishing: Heidelberg, Germany, 2015. [[CrossRef](#)]
26. Yin, Y.Y.; Tang, Q.H.; Liu, X.C.; Zhang, X.J. Water scarcity under various socio-economic pathways and its potential effects on food production in the Yellow River basin. *Hydrol. Earth Syst. Sci.* **2017**, *21*, 791–804. [[CrossRef](#)]
27. Cao, S.; Wang, X.; Song, Y.; Chen, L.; Feng, Q. International Journal of Applied Earth Observation and Geoinformation. *Ecol. Econ.* **2010**, *69*, 1454–1462. [[CrossRef](#)]
28. Farr, T.G.; Rosen, P.A.; Caro, E.; Crippen, R.; Duren, R.; Hensley, S.; Kobrick, M.; Paller, M.; Rodriguez, E.; Roth, L.; et al. The Shuttle Radar Topography Mission. *Rev. Geophys.* **2007**, *45*, RG2004. [[CrossRef](#)]
29. Breiman, L. *Classification and Regression Trees*; Routledge: London, England, 1984.
30. Gorelick, N.; Hancher, M.; Dixon, M.; Ilyushchenko, S.; Thau, D.; Moore, R. Google Earth Engine: Planetary-scale geospatial analysis for everyone. *Remote Sens. Environ.* **2017**, *202*, 18–27. [[CrossRef](#)]
31. Sedano, F.; Lisboa, S.; Duncanson, L.; Ribeiro, N.; Siteo, A.; Sahajpal, R.; Hurtt, G.; Tucker, C. Monitoring intra and inter annual dynamics of forest degradation from charcoal production in Southern Africa with Sentinel—2 imagery. *Int. J. Appl. Earth Obs. Geoinf.* **2020**, *92*, 102184. [[CrossRef](#)]
32. Huang, C.; Yang, Q.; Guo, Y.; Zhang, Y.; Guo, L. The pattern, change and driven factors of vegetation cover in the Qin Mountains region. *Sci. Rep.* **2020**, *10*, 20591. [[CrossRef](#)]
33. Jin, Z.; Azzari, G.; You, C.; Di Tommaso, S.; Aston, S.; Burke, M.; Lobell, D.B. Smallholder maize area and yield mapping at national scales with Google Earth Engine. *Remote Sens. Environ.* **2019**, *228*, 115–128. [[CrossRef](#)]
34. Oliphant, A.J.; Thenkabail, P.S.; Teluguntla, P.; Xiong, J.; Gumma, M.K.; Congalton, R.G.; Yadav, K. Mapping cropland extent of Southeast and Northeast Asia using multi-year time-series Landsat 30-m data using a random forest classifier on the Google Earth Engine Cloud. *Int. J. Appl. Earth Obs. Geoinf.* **2019**, *81*, 110–124. [[CrossRef](#)]
35. Pekel, J.F.; Cottam, A.; Gorelick, N.; Belward, A.S. High-resolution mapping of global surface water and its long-term changes. *Nature* **2016**, *540*, 418–422. [[CrossRef](#)]
36. Liu, D.; Duan, H.; Loisel, S.; Hu, C.; Zhang, G.; Li, J.; Yang, H.; Thompson, J.R.; Cao, Z.; Shen, M.; et al. Observations of water transparency in China's lakes from space. *Int. J. Appl. Earth Obs. Geoinf.* **2020**, *92*, 102187. [[CrossRef](#)]
37. Liu, X.; Hu, G.; Chen, Y.; Li, X.; Xu, X.; Li, S.; Pei, F.; Wang, S. High-resolution multi-temporal mapping of global urban land using Landsat images based on the Google Earth Engine Platform. *Remote Sens. Environ.* **2018**, *209*, 227–239. [[CrossRef](#)]
38. Liu, X.P.; Huang, Y.H.; Xu, X.C.; Li, X.C.; Li, X.; Ciais, P.; Lin, P.R.; Gong, K.; Ziegler, A.D.; Chen, A.N.; et al. High-spatiotemporal-resolution mapping of global urban change from 1985 to 2015. *Nat. Sustain.* **2020**, *3*, 564–570. [[CrossRef](#)]
39. Gong, P.; Liu, H.; Zhang, M.N.; Li, C.C.; Wang, J.; Huang, H.B.; Clinton, N.; Ji, L.Y.; Li, W.Y.; Bai, Y.Q.; et al. Stable classification with limited sample: Transferring a 30-m resolution sample set collected in 2015 to mapping 10-m resolution global land cover in 2017. *Sci. Bull.* **2019**, *64*, 370–373. [[CrossRef](#)]
40. Parente, L.; Mesquita, V.; Miziara, F.; Baumann, L.; Ferreira, L. Assessing the pasturelands and livestock dynamics in Brazil, from 1985 to 2017: A novel approach based on high spatial resolution imagery and Google Earth Engine cloud computing. *Remote Sens. Environ.* **2019**, *232*, 111301. [[CrossRef](#)]
41. Roy, D.P.; Wulder, M.A.; Loveland, T.R.; Woodcock, C.E.; Allen, R.G.; Anderson, M.C.; Helder, D.; Irons, J.R.; Johnson, D.M.; Kennedy, R.; et al. Landsat-8: Science and product vision for terrestrial global change research. *Remote Sens. Environ.* **2014**, *145*, 154–172. [[CrossRef](#)]

42. Markham, B.L.; Storey, J.C.; Williams, D.L.; Irons, J.R. Landsat sensor performance: History and current status. *IEEE Trans. Geosci. Remote Sens.* **2004**, *42*, 2691–2694. [\[CrossRef\]](#)
43. Masek, J.G.; Vermote, E.F.; Saleous, N.E.; Wolfe, R.; Lim, T.K. A Landsat surface reflectance dataset for North America, 1990–2000. *IEEE Geosci. Remote Sens. Lett.* **2006**, *3*, 68–72. [\[CrossRef\]](#)
44. Foga, S.; Scaramuzza, P.L.; Guo, S.; Zhu, Z.; Dilley, R.D.; Beckmann, T.; Schmidt, G.L.; Dwyer, J.L.; Joseph Hughes, M.; Laue, B. Cloud detection algorithm comparison and validation for operational Landsat data products. *Remote Sens. Environ.* **2017**, *194*, 379–390. [\[CrossRef\]](#)
45. Loveland, T.R.; Reed, B.C.; Brown, J.F.; Ohlen, D.O.; Zhu, Z.; Yang, L.; Merchant, J.W. Development of a global land cover characteristics database and IGBP DISCover from 1 km AVHRR data. *Int. J. Remote Sens.* **2000**, *21*, 1303–1330. [\[CrossRef\]](#)
46. Lück, W.; van Niekerk, A. Evaluation of a rule-based compositing technique for Landsat-5 TM and Landsat-7 ETM+ images. *Int. J. Appl. Earth Obs. Geoinf.* **2016**, *47*, 1–14. [\[CrossRef\]](#)
47. Flood, N. Seasonal Composite Landsat TM/ETM+ Images Using the Medoid (a Multi-Dimensional Median). *Remote Sens.* **2013**, *5*, 6481–6500. [\[CrossRef\]](#)
48. Azzari, G.; Lobell, D.B. Landsat-based classification in the cloud: An opportunity for a paradigm shift in land cover monitoring. *Remote Sens. Environ.* **2017**, *202*, 64–74. [\[CrossRef\]](#)
49. Dorren, L.K.A.; Maier, B.; Seijmonsbergen, A.C. Improved Landsat-based forest mapping in steep mountainous terrain using object-based classification. *For. Ecol. Manag.* **2003**, *183*, 31–46. [\[CrossRef\]](#)
50. Polykretis, C.; Grillakis, M.G.; Alexakis, D.D. Exploring the impact of various spectral indices on land cover change detection using change vector analysis: A case study of Crete Island, Greece. *Remote Sens.* **2020**, *12*, 319. [\[CrossRef\]](#)
51. Defries, R.S.; Townshend, J.R.G. NDVI-derived land cover classifications at a global scale. *Int. J. Remote Sens.* **1994**, *15*, 3567–3586. [\[CrossRef\]](#)
52. Zha, Y.; Gao, J.; Ni, S. Use of normalized difference built-up index in automatically mapping urban areas from TM imagery. *Int. J. Remote Sens.* **2010**, *24*, 583–594. [\[CrossRef\]](#)
53. Wilson, E.H.; Sader, S.A. Detection of forest harvest type using multiple dates of Landsat TM imagery. *Remote Sens. Environ.* **2002**, *80*, 385–396. [\[CrossRef\]](#)
54. Huete, A. A soil-adjusted vegetation index (SAVI). *Remote Sens. Environ.* **1988**, *25*, 295–309. [\[CrossRef\]](#)
55. Tucker, C.J. Red and photographic infrared linear combinations for monitoring vegetation. *Remote Sens. Environ.* **1979**, *8*, 127–150. [\[CrossRef\]](#)
56. Rouse, J.W., Jr.; Haas, R.H.; Schell, J.A.; Deering, D.W. Monitoring Vegetation Systems in the Great Plains with ERTS. In *Third Earth Resources Technology Satellite-1 Symposium. Volume 1*; NASA Special Publication: Washington, DC, USA, 1974; Volume 351, p. 309.
57. Lewis, R.J. An introduction to classification and regression tree (CART) analysis. In Proceedings of the 2000 Annual Meeting of the Society for Academic Emergency Medicine, San Francisco, CA, USA, 22–25 May 2000.
58. Olofsson, P.; Foody, G.M.; Herold, M.; Stehman, S.V.; Woodcock, C.E.; Wulder, M.A. Good practices for estimating area and assessing accuracy of land change. *Remote Sens. Environ.* **2014**, *148*, 42–57. [\[CrossRef\]](#)
59. Wulder, M.A.; White, J.C.; Magnussen, S.; McDonald, S. Validation of a large area land cover product using purpose-acquired airborne video. *Remote Sens. Environ.* **2007**, *106*, 480–491. [\[CrossRef\]](#)
60. Man, C.D.; Nguyen, T.T.; Bui, H.Q.; Lasko, K.; Nguyen, T.N.T. Improvement of land-cover classification over frequently cloud-covered areas using Landsat 8 time-series composites and an ensemble of supervised classifiers. *Int. J. Remote Sens.* **2017**, *39*, 1243–1255. [\[CrossRef\]](#)
61. Fu, H.; Chen, J. Formation, features and controlling strategies of severe haze-fog pollutions in China. *Sci. Total Environ.* **2017**, *578*, 121–138. [\[CrossRef\]](#)
62. Zhang, Y.; Guindon, B. Quantitative assessment of a haze suppression methodology for satellite imagery: Effect on land cover classification performance. *IEEE Trans. Geosci. Remote Sens.* **2003**, *41*, 1082–1089. [\[CrossRef\]](#)
63. Foody, G.M. Assessing the accuracy of land cover change with imperfect ground reference data. *Remote Sens. Environ.* **2010**, *114*, 2271–2285. [\[CrossRef\]](#)
64. Olofsson, P.; Foody, G.M.; Stehman, S.V.; Woodcock, C.E. Making better use of accuracy data in land change studies: Estimating accuracy and area and quantifying uncertainty using stratified estimation. *Remote Sens. Environ.* **2013**, *129*, 122–131. [\[CrossRef\]](#)
65. Zhao, Y.; Feng, D.; Yu, L.; Cheng, Y.; Zhang, M.; Liu, X.; Xu, Y.; Fang, L.; Zhu, Z.; Gong, P. Long-Term Land Cover Dynamics (1986–2016) of Northeast China Derived from a Multi-Temporal Landsat Archive. *Remote Sens.* **2019**, *11*, 599. [\[CrossRef\]](#)
66. Bontemps, S.; Defourny, P.; Radoux, J.; Van Bogaert, E.; Lamarche, C.; Achard, F.; Mayaux, P.; Boettcher, M.; Brockmann, C.; Kirches, G. Consistent global land cover maps for climate modelling communities: Current achievements of the ESA's land cover CCI. In Proceedings of the ESA Living Planet Symposium, Edimburgh, UK, 9–13 September 2013; pp. 9–13.
67. Tassi, A.; Vizzari, M. Object-Oriented LULC Classification in Google Earth Engine Combining SNIC, GLCM, and Machine Learning Algorithms. *Remote Sens.* **2020**, *12*, 3776. [\[CrossRef\]](#)
68. Riad, P.; Graefe, S.; Hussein, H.; Buerkert, A. Landscape transformation processes in two large and two small cities in Egypt and Jordan over the last five decades using remote sensing data. *Landsc. Urban Plan.* **2020**, *197*, 103766. [\[CrossRef\]](#)
69. Li, J.; Peng, S.; Li, Z. Detecting and attributing vegetation changes on China's Loess Plateau. *Agric. For. Meteorol.* **2017**, *247*, 260–270. [\[CrossRef\]](#)

70. Guo, J.; Gong, P. Forest cover dynamics from Landsat time-series data over Yan'an city on the Loess Plateau during the Grain for Green Project. *Int. J. Remote Sens.* **2016**, *37*, 4101–4118. [[CrossRef](#)]
71. Song, C.H.; Zhang, Y.L.; Mei, Y.; Liu, H.; Zhang, Z.Q.; Zhang, Q.F.; Zha, T.G.; Zhang, K.R.; Huang, C.L.; Xu, X.N.; et al. Sustainability of Forests Created by China's Sloping Land Conversion Program: A comparison among three sites in Anhui, Hubei and Shanxi. *For. Policy Econ.* **2014**, *38*, 161–167. [[CrossRef](#)]
72. Cao, S.X.; Xu, C.G.; Chen, L.; Wang, X.Q. Attitudes of farmers in China's northern Shaanxi Province towards the land-use changes required under the Grain for Green Project, and implications for the project's success. *Land Use Policy* **2009**, *26*, 1182–1194. [[CrossRef](#)]
73. Fu, B.; Chen, L.; Ma, K.; Zhou, H.; Wang, J. The relationships between land use and soil conditions in the hilly area of the loess plateau in northern Shaanxi, China. *Catena* **2000**, *39*, 69–78. [[CrossRef](#)]
74. Feng, Q.; Zhao, W.; Fu, B.; Ding, J.; Wang, S. Ecosystem service trade-offs and their influencing factors: A case study in the Loess Plateau of China. *Sci. Total Environ.* **2017**, *607–608*, 1250–1263. [[CrossRef](#)]
75. Wang, F.; Liang, W.; Fu, B.; Jin, Z.; Yan, J.; Zhang, W.; Fu, S.; Yan, N. Changes of cropland evapotranspiration and its driving factors on the loess plateau of China. *Sci. Total Environ.* **2020**, *728*, 138582. [[CrossRef](#)] [[PubMed](#)]
76. Yang, M.; Wang, S.; Zhao, X.; Gao, X.; Liu, S. Soil properties of apple orchards on China's Loess Plateau. *Sci. Total Environ.* **2020**, *723*, 138041. [[CrossRef](#)]
77. Tang, Q.; Bennett, S.J.; Xu, Y.; Li, Y. Agricultural practices and sustainable livelihoods: Rural transformation within the Loess Plateau, China. *Appl. Geogr.* **2013**, *41*, 15–23. [[CrossRef](#)]
78. Xu, Z.; Chau, S.N.; Chen, X.; Zhang, J.; Li, Y.; Dietz, T.; Wang, J.; Winkler, J.A.; Fan, F.; Huang, B.; et al. Assessing progress towards sustainable development over space and time. *Nature* **2020**, *577*, 74–78. [[CrossRef](#)]
79. Ouyang, Z.; Zheng, H.; Xiao, Y.; Polasky, S.; Liu, J.; Xu, W.; Wang, Q.; Zhang, L.; Xiao, Y.; Rao, E.; et al. Improvements in ecosystem services from investments in natural capital. *Science* **2016**, *352*, 1455–1459. [[CrossRef](#)] [[PubMed](#)]
80. Liu, Y.S.; Fang, F.; Li, Y.H. Key issues of land use in China and implications for policy making. *Land Use Policy* **2014**, *40*, 6–12. [[CrossRef](#)]
81. Liu, J.; Liu, M.; Tian, H.; Zhuang, D.; Zhang, Z.; Zhang, W.; Tang, X.; Deng, X. Spatial and temporal patterns of China's cropland during 1990–2000: An analysis based on Landsat TM data. *Remote Sens. Environ.* **2005**, *98*, 442–456. [[CrossRef](#)]
82. Liu, L.; Xu, X.; Chen, X. Assessing the impact of urban expansion on potential crop yield in China during 1990–2010. *Food Secur.* **2015**, *7*, 33–43. [[CrossRef](#)]
83. Zheng, H.X.; Zhang, L.; Zhu, R.R.; Liu, C.M.; Sato, Y.; Fukushima, Y. Responses of streamflow to climate and land surface change in the headwaters of the Yellow River Basin. *Water Resour. Res.* **2009**, *45*, 641–648. [[CrossRef](#)]
84. Li, J.; Liu, D.; Wang, T.; Li, Y.; Wang, S.; Yang, Y.; Wang, X.; Guo, H.; Peng, S.; Ding, J.; et al. Grassland restoration reduces water yield in the headstream region of Yangtze River. *Sci. Rep.* **2017**, *7*, 2162. [[CrossRef](#)] [[PubMed](#)]